Magnetic field optimization of permanent magnet undulators for arbitrary polarization

J. Bahrdt[a],*, W. Frentrup[a], A. Gaupp[a], M. Scheer[a], U. Englisch[b]

[a] BESSY GmbH Experiments, Albert-Einstein-Str. 15, D-12489 Berlin, Germany
[b] Max-Planck-Institut für Metallforschung, Heisenbergstr. 3, D-70569 Stuttgart, Germany

Abstract

Techniques for improving the magnetic field quality of APPLE II undulators are discussed. Individual block characterization including the inhomogeneities of the magnetization permits a precise prediction of field integrals as required for sorting. Specific shimming procedures adapted to the magnetic design of APPLE II undulators have to be employed in order to meet the stringent requirements of insertion devices in third generation synchrotron radiation sources as demonstrated for BESSY.
© 2003 Elsevier B.V. All rights reserved.

1. Introduction

Controllable polarization provides important and crucial information about the sample in experiments using short wavelength synchrotron radiation. The magnetic circular dichroism, for example, is extensively used to study magnetic properties of materials potentially suitable for data storage. This method as well as investigations of samples with chiral symmetry require tunable circularly polarized radiation. The magnetic linear dichroism provides information about anti-ferro-magnetic materials and systems that hold promises for data storage, as well. These investigations and many others that use polarization to extract spatial information (e.g. angle resolved photo emission) require linear polarization with controllable orientation. A range of rotation of 180° (instead of 90°) is needed when the orientation of the sample cannot be changed and its intrinsic orientation is not known.

Insertion devices of the APPLE II type [1] are presently preferred in many synchrotron radiation facilities because the highest horizontal field among all planar helical undulators is achieved. These devices consist of four rows of permanent magnets that can be shifted longitudinally with respect to each other. Linear superposition of fields generated by these rows results in the desired magnetic field distribution.

*Corresponding author. Tel.: +49-30-6392-4657; fax: +49-30-6392-2989.

E-mail address: bahrdt@bessy.de (J. Bahrdt).

The required field quality of such undulators to be operated in third generation synchrotron radiation sources causes stringent specifications. They have to be met although the quality of commercially available magnets is not yet adequate with respect to both the magnetic and geometric properties in order to build a device without magnet sorting and shimming. This paper discusses magnet sorting (Section 3) and shimming (Sections 4–7) strategies which have successfully been used at BESSY to meet the requirements. Many aspects are also relevant for in-vacuum undulators where conventional shimming is not applicable.

2. Undulators at BESSY

At the time of writing (March 2003), BESSY has four APPLE II type devices in operation and a fifth APPLE II device (UE49) is under construction (Table 1). Two UE56 devices are double undulators which are optimized for fast helicity switching (up to 100 Hz) [2]. An UE46 and an UE52 permits a continuous inclination of the linear polarization from $0°$ to $90°$. The UE49 has four shiftable magnet rows and thus extends this range to $180°$.

All BESSY APPLE II devices have been characterized by soft X-ray polarimetry [3]. The degree of polarization (elliptical or linear under variable angles) for different shifts (relative longitudinal positions between magnet rows) agree with the prediction within its error bars.

Table 1
APPLE II devices built at BESSY

Device	λ(mm)	Periods
UE56-1	56	2×30
UE56-2	56	2×30
UE46	46	70
UE52	52	77
UE49	49	63
PSI-UE56	56	2×30

The PSI-UE56, installed at the Swiss Light Source, has been designed and built in close cooperation with BESSY.

3. Magnet sorting

Sorting, i.e., distributing blocks or magnetic subassemblies inside the magnetic structure according to the available knowledge of the magnetic (and geometric) properties, can be done at four stages at least during the assembly:

(1) Individual blocks are sorted based on single block measurements;
(2) subassemblies holding several magnets are sorted according to measurements of these units;
(3) during assembly intermediate measurements are made to resort the remaining units;
(4) subassemblies are rearranged within the undulator based on measurements of the completed structure (in situ-sorting [4]).

It has been demonstrated at BESSY that steps 1 and 2 are sufficient once a detailed and accurate magnetic characterization has been performed.

Two types of data sets are needed to describe magnet blocks or subassemblies: (1) The integrated dipole moment (magnitude and orientation). The three components are adequate for hybrid undulators but not sufficient for APPLE II type undulators. (2) A map of fields or field integrals describing the inhomogeneities.

At BESSY, the dipole moments of single blocks are determined in an automated Helmholtz coil system with a reproducibility of 0.05% r.m.s. for the magnitude of the dipole moment. The uncertainty in the orientation of the dipole is $0.06°$ r.m.s. Typical errors of die pressed magnets are below 0.3% r.m.s. for the magnitude and below $0.3°$ r.m.s. for the orientation of the dipole moment. The geometrical tolerances of the magnets have a significant influence on the width of the error distribution.

Block inhomogeneities are characterized with a stretched wire system: At a distance of 8 mm with respect to a straight wire which corresponds to half the minimum gap a magnet is moved in steps of 2.5 mm while the voltage induced in the wire of 125 μm diameter is monitored. The relative orientation of the magnet and wire mimics the situation in the undulator [2] where the wire

represents the electron beam. Only those magnet surfaces have been characterized which can face the midplane. That are four sides for the long-itudinally (A-magnets) and two sides for the vertically (B-magnets) magnetized blocks. A repeatability of 0.0004 Tmm r.m.s. is achieved for blocks with magnetization parallel to the wire (type A), and of 0.002 Tmm r.m.s. for blocks with magnetization perpendicular to the wire (type B).

The field integrals of die pressed magnets delivered from various suppliers (Vacuum-schmelze, Sumitomo, Shin-Etsu, Magnequench) have been studied with the BESSY system. The data of all suppliers are comparable and are within a band of ± 0.05 Tmm (peak to peak).

A rotating coil (5 Hz) and a lock-in amplifier provide similar information about magnet inho-mogeneities with an accuracy of 0.001 Tmm as described by Tanaka et al. [5]. These data permit a reliable prediction of field integrals of a 10 period planar undulator [5].

At BESSY both the Helmholtz coil data and the stretched wire data are used in a simulated annealing code [6]. The cost function is a weighted sum of the field integrals and of the phase errors [7].

Die pressed magnets can have a systematic inhomogeneity pattern. This is particular notice-able in case of UE56 when imperfections of the magnetic block pressing caused field errors that add up without cancellations [2]. To cope with this problem adjacent periods can be equipped with two magnet types which differ in the orientation of the magnetization with respect to the pressing direction. This has successfully been done in the case of the BESSY-UE52 and the PSI-UE56 [8] undulators.

In the following the optimization procedure of the 77 period UE52 APPLE II undulator is described. The improvement in the field quality was made possible by a sorting procedure that is based on a detailed magnet characterization and by controlling all geometric tolerances.

After magnet sorting (based on dipole and inhomogeneity data) two adjacent magnets were glued into a common keeper. The keepers were re-measured magnetically with a stretched wire and geometrically with a coordinate measuring ma-

chine. Field integral predictions for the complete device due to these keeper data are basically the same as predictions based on single block data. This finding indicates that a sufficient geometrical accuracy is achieved. Typical errors in the gluing process are 40 μm r.m.s. for displacement and 1 mrad r.m.s. for tilt. Nevertheless, a few keepers were re-located to compensate for gluing toler-ances. Then, the keepers were mounted onto the I-beams without any further measurements and resorting during assembly.

In the top part of Fig. 1 the straight line integrals (integrated along a line parallel to the axis from $-\infty$ to x) for the prediction and for the measurement of the complete undulator are compared. A summation of the stretched wire data of the keeper measurements from the begin-ning of the undulator to a particular position provide the predicted data. The measured data are obtained with a scanning Hall probe. The pre-dicted and measured integrals are evaluated along
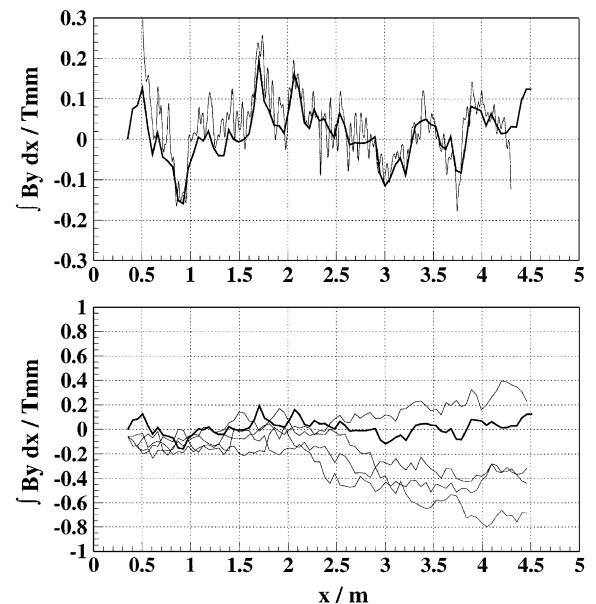

Fig. 1. Top: Predicted vertical field integrals (integrated along a line parallel to the axis from $-\infty$ to x) for the UE52 at gap = 16 mm, shift = 0 mm and $z = 20$ mm (thick line) are compared to Hall probe data (thin line). The periodic part of the Hall probe data has been filtered out. Bottom: Predicted field integrals for the UE52 ($z = 20$ mm) for the sorted (thick line) and a few random (thin line) configurations.
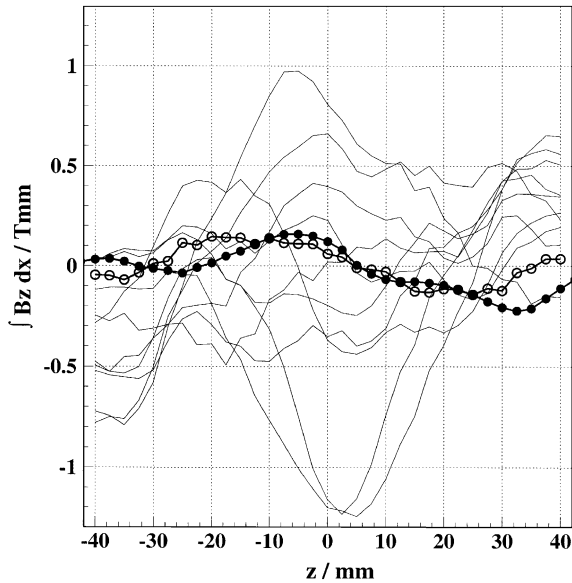
Fig. 2. Transverse distribution of the horizontal field integrals (integrated in x from $-\infty$ to $+\infty$) of the completed UE52 at gap $= 16$ mm and shift $= 0$ mm. Open circles: prediction of the sorted configuration; full circles: measurement; thin line: predictions for several unsorted configurations.

a line horizontally displaced from the axis by 20 mm. At this location the magnetic effect of a transverse keeper displacement (assembling error) is minimized. The two data sets correlate well and differences below ± 0.15 Tmm are noted (except for the end pole region). Excellent agreement between prediction and measurement has been found also at $z = -20$ mm for $\int B_y$ and at $z = 0$ mm for $\int B_z$. The terms $\int B_y|_{z=0 \text{ mm}}$ and $\int B_z|_{z=\pm 20 \text{ mm}}$ have not been measured before shimming. Unsorted magnet block distributions yield significantly larger field integrals (Fig. 1 bottom part).

Fig. 2 compares predicted and measured transverse distributions of integrals parallel to the axis from $x = -\infty$ to $+\infty$. The measurements have been obtained with a 6 m long, moving stretched wire system sensing the field distribution in the undulator region. The wire was moved in steps of 2.5 mm. Again, a good agreement between prediction and reality is observed. For comparison, integrals of 10 different randomly selected magnet configuration are shown demonstrating the efficiency of the sorting procedure.

Including the inhomogeneity data into the calculation for prediction is crucial to achieve such a good agreement. Simulations show that for a small gap of 16 mm the field integrals predicted from dipole data alone and from data including the stretched wire differ drastically. The block inhomogeneities dominate the field quality. The relative importance of dipole and higher order errors certainly changes with gap because of the different dependence of higher multipoles with distance.

The measurements plotted in Figs. 1 and 2 formed the basis for the succeeding shimming procedure. As shown below (see Section 7), the field integrals based on sorting must be small enough (of the order of ± 0.1 Tmm) before shimming is started. It is useful when keepers of the assembled undulator can be arbitrarily repositioned. Stretched wire data of the keepers are used in this process.

So far, the BESSY design was such that keepers could only be exchanged within two rows located diagonally. In the future UE49, it will be possible to allocate any keeper to any row. This additional symmetry will give more flexibility for in situ-sorting and will thus improve the field quality prior to shimming.

A large-scale production of undulators for FELs requires a fast block characterization. E.g. Measuring and sorting of keepers carrying two magnets (the magnets are randomly distributed to the keepers) reduces the measurement time by a factor of 6 as compared to an individual block characterization whereas the field integrals and phase errors increase only by a factor of about 1.2. Even larger factors can be tolarated for a single pass FEL because it is less sensitive to multipole and phase errors than a storage ring and hence larger modules than magnet pairs can be used.

4. On-axis trajectory shimming

Shimming here means the addition (or removal) of magnetic material to (or from) the structure such that the field quality improves. Shims may be ferromagnetic (i.e. small pieces of iron) or permanently magnetic (i.e. small pieces of NdFeB). Field

quality refers to the straightness of the on-axis trajectory, the optical phase jitter [7], and integrated multipoles. The first two criteria are not independent from each other since minimum phase jitter can only be achieved for a straight trajectory. Shimming should ultimately lead to a brilliance of the radiation not limited by magnetic field properties but by electron beam emittance and energy spread. The minimization of multipoles is essential for unperturbed storage ring operation.

Conventional shimming techniques [9] where thin soft iron shims are placed on top of the magnets are not applicable for an APPLE II because no shims can be located at the center, and because iron shims change their response function during row shifting (iron shims can, however, be used to compensate shift-dependent field integrals, see Section 6). The intentional transverse and

vertical displacement of magnets and/or keepers, called "virtual shimming", is done in many laboratories [10]. This technique enables one to manipulate the on-axis fields and, to a certain extent, to reduce the multipoles (Fig. 3). The keepers of the BESSY devices are mounted on laminated stainless steel spacers. Peeling off foils of 25 μm thickness provides the flexibility to adjust the keeper in both transverse directions.

After virtual shimming, the jitter of the UE46 and the UE52 on-axis trajectories for all gaps remains within a band of 30 Tmm^2 for both field components (excluding endpole kicks which are compensated using additional coils).

5. Phase optimization

After straightening the on-axis trajectory by virtual shimming, the phase errors for the horizontal (vertical) linear polarization mode of the UE52 and UE46 devices are $3.4°$ $(4.2°)$ and $3.4°$ $(3.8°)$ r.m.s. respectively. Thus, no explicit phase shimming has been done. Part of the UE52 phase error is related to a slightly different gap setting of the two independent undulator sections (see below). The technique of virtual shimming is suitable to further improve these values as well as the trajectory straightness, if necessary.

Simulations show that phase errors below a few degrees for the first harmonic require systematic gap errors well below 20 μm. Systematic gap changes are introduced by fabrication errors and by I-beam bending due to the magnetic load.

The flatness of I-beams is typically 50 μm. The laminated spacers between I-beam and keepers are used to compensate for the measured height variation of the I-beam. Though the nominal spacer gradation is 25 μm an accuracy below 10 μm could be achieved by appropriate spacer sorting. The I-beams must be sufficiently stiff such that the remaining bending due to the magnetic forces can be tolerated.

In case of UE46 the I-beam has a length of 3.4 m. The bending could be limited to 5 μm by a modified mechanical design where the I-beam is supported at four points (using two cross bars) instead of two points as usual (at the expense of
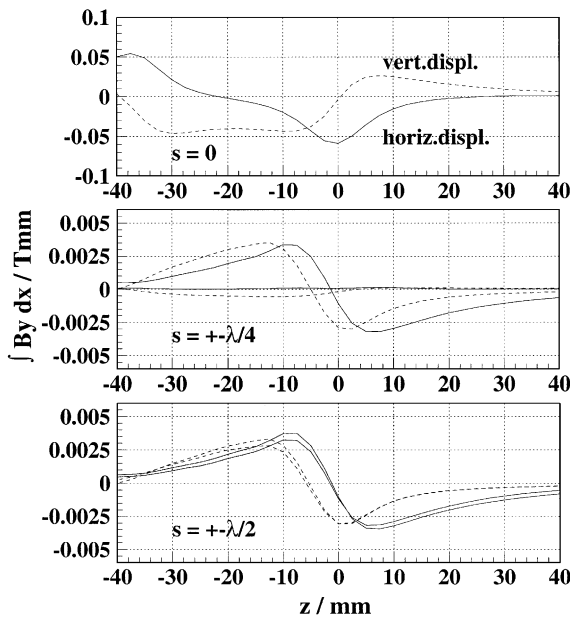

Fig. 3. Top: UE52 field integrals (gap = 16 mm) introduced by a horizontal (solid line) and a vertical (dashed line) keeper movement of 0.2 mm (virtual shimming) (each keeper carries one A- and one B-magnet). Middle and bottom: Shift dependence of field integrals introduced by virtual shimming for shifts of $s = \pm\lambda/4$ and $\pm\lambda/2$. The shift-dependent terms are derived by subtracting the field integrals at $s \neq 0$ from field integrals at $s = 0$. The solid and dashed lines refer to horizontal and vertical keeper displacements by 0.2 mm, respectively.

additional hinges). The UE52 has a total magnetic length is 4.2 m. To simplify fabrication the magnetic structure is divided longitudinally into two 2.1 m long I-beams motorized separately in gap and shift. Hence, two supporting points for each I-beam section are sufficient.

The gap reading must match the requirements with respect to resolution, reproducibility, and relative calibration. Each I-beam is actuated by two servo-motors operated in a feedback loop with optical linear encoders measuring the gap between the I-beams with a resolution of 100 nm. Presently, only one encoder per motor located about 300 mm off axis is used. This leads to measurement errors due to a beam roll around the longitudinal axis. For an accurate gap reading provision is made for additional linear encoders symmetrically located at the opposite side to derive an averaged value for the positioning feedback loop. For the next APPLE II device (UE49) the linear encoders will be placed at the undulator ends above the electron beam which will eliminate this kind of error.

Any gap taper is eliminated using the magnetic field as measured with a Hall probe. The relative setting of the four encoders is done by minimizing the residual phase advance. This technique has a sensitivity of 2µm.

6. Shift-dependent field integrals

It is observed that field integrals depend on row shift. This is due to the relative permeability deviating from unity. Typical values for the permeability of NdFeB magnets are $\mu_{\parallel} = 1.06$ and $\mu_{\perp} = 1.17$. The intended field changes due to row shift change the magnetization of blocks which in turn modifies the field.

A major contribution to the shift dependence of the field integrals may originate from the endpole regions [11]. This effect, however, can be minimized with a proper magnetic design [12].

Additionally, shift-dependent contributions are observed which originate from the periodic part. Displacing the blocks transversely, the two types of magnets differ in their signature of shift depending fields: The contributions from A-magnets (definition see above) are maximum near

shift $= \pm \lambda/4$ and are anti-symmetric with respect to shift $= 0$. The contributions from B-magnets are maximum near shift $= \pm \lambda/2$ and are symmetric with respect to shift $= 0$. These effects are based on the magnetization ($\mu \neq 1$) of a thin magnet sheet with the thickness equal to the block displacement by B-magnets located at the neighbouring magnet row. The symmetry of the B-magnets on one row with respect to an A- or B-magnet on the other row is different and, hence, the signatures of A- or B-magnet displacements differ.

Before virtual shimming, the UE52 device had horizontal and vertical shift-dependent field integrals of the order of 0.03 Tmm after subtracting the endpole contribution (using RADIA model calculations [13], see Fig. 4). Other APPLE II devices (UE46 and PSI-UE56-1/2) showed effects up to 0.08 Tmm. These shift-dependent integrals can partially be explained by a random
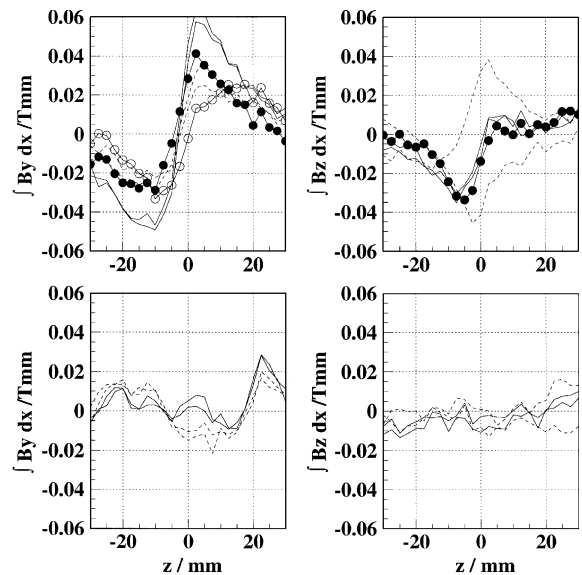

Fig. 4. Shift-dependent field integrals (gap = 16 mm) of the UE52 (after virtual shimming) before (top) and after (bottom) shimming with Fe-shims. Data for $s = \pm \lambda/2$ (solid line) and $s = \pm \lambda/4$ (dashed line) are presented. Additionally, the shift-dependent terms before virtual shimming for $s = \lambda/2$ are given (full circles). Obviously, the virtual shimming procedure modified the shift-dependent terms. Removing the endpole effect with RADIA simulations the contribution from the periodic part becomes visible (open circles).

displacement of magnets. The UE52 device has magnet displacement errors of $\sigma_{\Delta_{y/z}} = 40$ μm. Assuming a normal distribution of these errors, only 30% (50%) of the vertical (horizontal) field differences can be explained. Another contribution may be a fluctuation of $\mu_{\parallel}$ and $\mu_{\perp}$ between magnet blocks. Quantitative data, however, are not available at this time.

Virtual shimming causes shift-dependent field integrals shown in Fig. 3 as predicted by RADIA model calculations.

Shift-dependent field integrals can be manipulated by introducing material with a large permeability. Fig. 5 shows the shift-dependent effects of iron shims located on top of the magnets as modelled by RADIA. The amplitude of the effect drops significantly at larger distances from the ID-center because the mutual magnetization of the neighboring magnet rows decreases.

The signature depends on the magnet type on which the shim is placed. The response of shims on A-magnets (A-shims) is antisymmetric with respect to shift = 0 whereas the response of B-shims is symmetric with respect to shift = 0.

The measured shift-dependent field integrals $\int B_{x/z} \, dx|_s$ are decomposed into symmetric and antisymmetric terms where y and z denote the vertical and transverse coordinate and s is the magnet row shift:

$$\int \Delta B_{y/z}^{\lambda/2} \, dx = \frac{1}{2} \left(\int B_{y/z} \, dx|_{s=\lambda/2} + \int B_{y/z} \, dx|_{s=-\lambda/2} \right) - \int B_{y/z} \, dx|_{s=0} \tag{1}$$

$$\int \Delta B_{y/z}^{\lambda/4} \, dx = \frac{1}{2} \left(\int B_{y/z} \, dx|_{s=\lambda/4} - \int B_{y/z} \, dx|_{s=-\lambda/4} \right). \tag{2}$$

The term $\int \Delta B_{y/z}^{\lambda/2} \, dx$ in Eq. (1) is minimized using B-shims. Thereafter, $\int \Delta B_{y/z}^{\lambda/4} \, dx$ in Eq. (2) is minimized using A-shims which do not influence the term $\int \Delta B_{y/z}^{\lambda/2} \, dx$ (cf. Fig. 5) because at $s = 0$ and $\lambda/2$ no B-magnet faces the A-magnet.

The iron shims are glued on top of the structure. This is a compromise and no perfect compensation can be expected. Ideally, one would have to place also material inside the air gap between the rows to compensate for the horizontal virtual shimming and inside the magnet bulk to compensate for the $\mu_{\parallel}$ and $\mu_{\perp}$ fluctuation. Fig. 4 shows the shift-dependent field integrals of the UE52 device before (top) and after applying iron shims (bottom). An improvement of a factor of six within a region of ± 20 mm justifies the effort.

7. Shift-independent field integrals

Strong field integrals of ± 3 Tmm have been observed at the BESSY-UE56 undulators which are due to magnet inhomogeneities (see Section 3 and Fig. 6). They have been compensated with permanent magnet shims located on top of the magnets inside the periodic part sacrificing 1 mm of gap. For all other APPLE II-IDs an improved fabrication and sorting scheme resulted in a
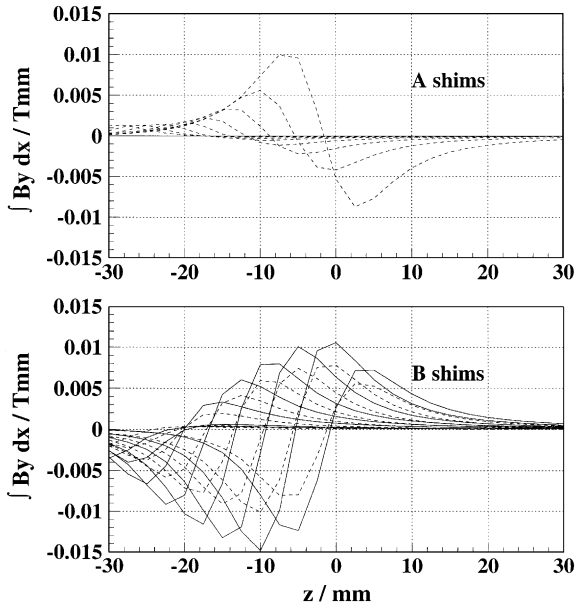

Fig. 5. Shift dependence of UE52 field integrals (gap = 16 mm) of Fe-shims on A-magnets (top) and B-magnets (bottom) at various transverse positions as modelled with RADIA (see caption Fig. 3 for definition). Data are given for shifts of $s = \lambda/2$ (solid line) and $s = \lambda/4$ (dashed line). For negative shifts the data of A-shims reverse sign whereas the data of B-shims do not.

reduction of the field integrals of the unshimmed devices by about a factor of 10. For these devices we designed permanent magnet arrays which are located at both ends of the undulator (Fig. 7)
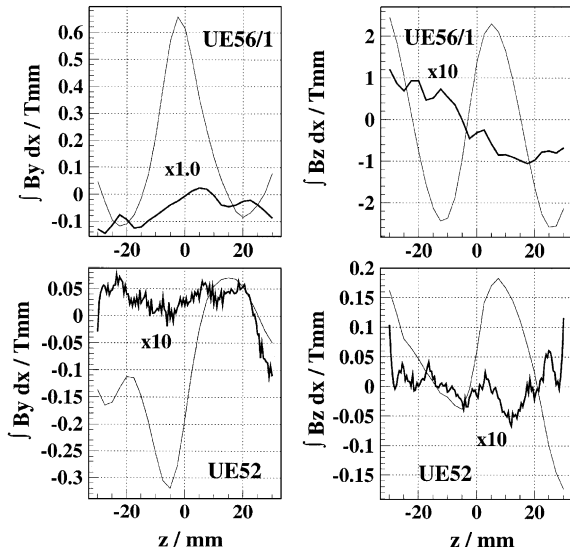

Fig. 6. Field integrals of the UE56-1 (upstream module) (top) and of the UE52 (bottom) at minimum gap of 16 mm before (thin line) and after (thick line) shimming. When indicated the residual field integrals after shimming have been enhanced by a factor of 10. The measurement step size is 2.5 mm (top) and 0.5 mm (bottom). The lower graphs show averaged data derived from 9 individual scans.

similar to the ALS-"multiple trim magnets" [14]. The rational for the layout is discussed in the appendix. The grid (and block) size is 4 mm (one quarter of the minimum gap). The magnets are quadratic and can be assembled in two orientations (magnetic vector pointing vertically or horizontally). The magnet strength can be adjusted independent of the vertical position and hence the shape of the response function is independent of the strength. For that purpose, we wire-cut columns of 4×4 mm^2 cross-section with transverse magnetization. The longitudinal dimension of these columns varies in steps of 0.1 mm. The magnets can be shifted vertically for a fine strength adjustment or for tuning the line width of the response function. In the appendix, it is shown that the strength of the residual oscillations is expected to be about $\pm 0.5\%$ to $\pm 1\%$ of the error field for the given grid of shims.

Fig. 6 presents field integrals of the UE56-1 upstream module and of the UE52. The amplitudes of the oscillations are about ± 0.02 and ± 0.002 Tmm, respectively, which is roughly 1% of the amplitudes before shimming. It turns out that the high spatial frequency part cannot be reduced much further. It is observed that the residual fields of the UE56-1 are significant [15] for the storage ring (skew octupole component) whereas the residual fields of the UE52 are not. This defines the strategy for optimization: Field
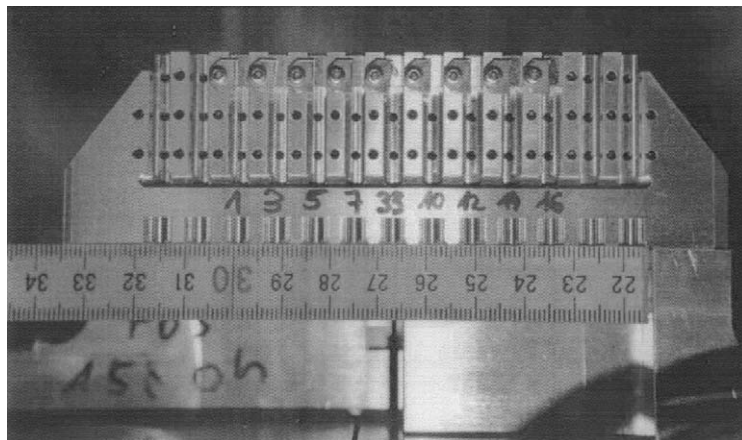

Fig. 7. "Magic fingers" of the UE52. The permanent magnets are clamped into the vertical slots. At the backside of this device another array of slots is available. It is displaced horizontally by 4 mm with respect to the slots at the front.

integral shimming in the described way must not be started unless the field integrals are of the order of 0.1 Tmm. Then, the target values for the field integrals of 0.01 Tmm can be achieved via shimming. For the UE56 this was not the case. Here, a different technique might be applicable. To overcome the problem of discretization continuously wire-cut magnets (a proven technique for NdFeB-material) can be used which are shaped appropriately and mounted on either end of the device.

8. Conclusion

It has been shown that the magnet field quality concerning trajectory, phase and multipole errors of APPLE II undulators can reach a level comparable to planar devices. Trajectory straightening can easily be done with virtual shimming. Phase errors were already acceptable after trajectory straightening which is the result of sorting and precision mounting.

The minimization of the field integrals is documented in Table 2. Field integral predictions from sorting agree well with measurements within ± 0.15 Tmm. Magnet sorting based on block inhomogeneities improves the quality by about one order of magnitude compared to a random distribution. Shift-independent terms are reduced by a factor of 50 with an array of permanent magnets at the undulator ends. Shift-dependent field integrals are reduced by a factor of six using iron shims.

Each individual block of the BESSY devices has been characterized. This was essential in order to develop appropriate measurement tools and to study the block quality. Based on these data, details about the manufacturing process can be deduced and the results might help to improve the magnet properties in the future. For an undulator production, it is sufficient to characterize the inhomogeneities of subassemblies consisting of several magnets.

An efficient sorting procedure as described above is crucial for several reasons. Sorting of subassemblies is necessary because it reduces field integrals to a low level where additional shimming produces only weak oszillations in the residual field integrals. In case of in-vacuum undulators a reliable sorting procedure is of utmost importance because conventional shimming is not possible. Regarding a mass production of undulators for a SASE FEL an iterative measurement and sorting during assembly can be omitted which helps to minimize time and cost.

Appendix A

An arbitrary field integral distribution can be written as a convolution of the magnetization distributions m_y and m_z with two generic functions g and h:

$$
\int_{-\infty}^{+\infty} dx\, B_{y/z}(y, z)
$$
$$
= \int_{y_{\min}}^{y_{\max}} dy_0 \int_{z_{\min}}^{z_{\max}} dz_0
$$
$$
\pm m_{y/z}(y_0, z_0)\, g(y - y_0, z - z_0)
$$
$$
+ m_{z/y}(y_0, z_0)\, h(y - y_0, z - z_0). \tag{A.1}
$$

Table 2
Field integrals within a transverse region of ± 20 mm at a gap of 16 mm (8 mm distance in case of single block data)

	Field integrals (peak to peak) (Tmm)	Device
	± 0.05	Single blocks
Systematic errors	± 3.0	UE56/1/2
Random errors	± 1.0	UE52
Prediction from sorting	± 0.15	UE52
Real device after sorting	± 0.15	UE52
After shimming	± 0.004	UE52
Shift dependence	± 0.06	UE52
After shimming	± 0.01	UE52

g and h are defined via the field integrals of a point dipole located at (y_0, z_0).

$$\int_{-\infty}^{+\infty} \mathrm{d}x\, B_{y/z}^{\mathrm{dipole}}(y, z)$$

$$= \pm \left(\frac{M_{y/z}\, \tilde{y}^2}{\pi(\tilde{y}^2 + \tilde{z}^2)^2} - \frac{M_{y/z}}{2\pi(\tilde{y}^2 + \tilde{z}^2)} \right) + \frac{M_{z/y}\, \tilde{y}\, \tilde{z}}{\pi(\tilde{y}^2 + \tilde{z}^2)^2}$$

$$= \pm M_{y/z}\, g(\tilde{y}, \tilde{z}) + M_{z/y}\, h(\tilde{y}, \tilde{z}) \qquad (A.2)$$

with $\tilde{y} = y - y_0$ and $\tilde{z} = z - z_0$. Eq. (A.2) can be rewritten in complex form

$$\vec{B}^{i*} = \vec{M}(g + i\,h) \qquad (A.3)$$

where B^i is the field integral. Obviously, the "easy axis rotation theorem" which has been derived for infinitely wide magnet blocks [16] is valid also for field integrals of point dipoles. Dipole fields in 3D follow the less general "easy axis symmetry principle" [17].

In the following discussion, we assume that the field errors are located above midplane in a thin layer at a fixed $\tilde{y}$. The conclusions are valid also for the general case of vertically distributed errors.

The Fourier transforms $F(g)$ and $F(h)$ of g and h are correlated (subscripts denote the real and imaginary part).

$$F(g)_r = F(h)_i \qquad (A.4)$$

$$F(g)_i = F(h)_r = 0. \qquad (A.5)$$

For multipole shimming Eq. (A.1) has to be solved for m_y and m_z. With B_y^i being the field integral in Eq. (A.1) the Fourier transform of Eq. (A.1) is

$$F(B_y^i)/F(g)_r = F(m_y) + i\,F(m_z). \qquad (A.6)$$

This equation has no unique solution. The measured data can be reproduced either with a pure m_y or m_z distribution or with a combination of both as follows:

$$m_y = F^{-1}(F(B_y^i)/F(g)_r) \qquad (A.7)$$

$$m_z = F^{-1}(F(B_y^i)/(i\,F(g)_r)). \qquad (A.8)$$

Neither additional data at different y-locations nor the data $F(B_z)$ provide a further constraint as

$$F(B_y^i)_r = F(B_z^i)_i \qquad (A.9)$$
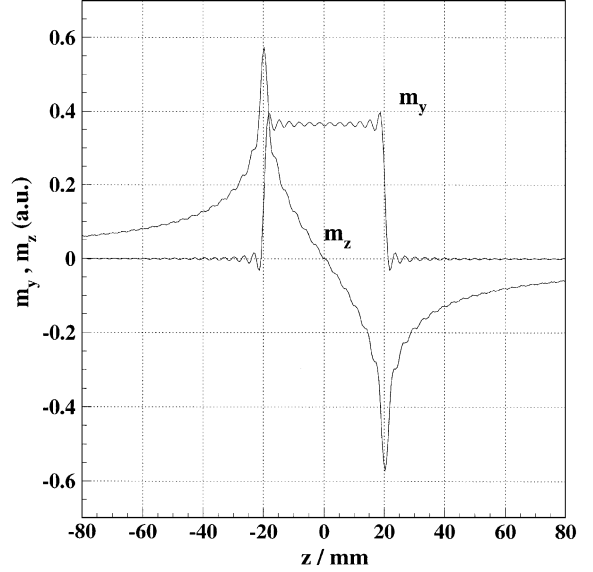
$$F(B_y^i)_i = -F(B_z^i)_r. \qquad (A.10)$$

Fig. 8. Deconvolution of field integrals for a rectangular distribution of m_y between $z = \pm 20$ mm using Eq. (A.7) (m_y) and Eq. (A.8) (m_z). The oscillations originate from the truncation of the arguments in Eqs. (A.7) and (A.8) prior to back transformation.

Distribution (A.7) and (A.8) can extend in z-direction far beyond the region of the magnetic material (see Fig. 8). A confinement of the m_y- and m_z-distribution to a finite transverse region (i.e. the width of the magnetic array) removes the ambiguity because the scaling of g and h is different for large $z(1/z^2$ vs. $1/z^3)$. For practical reasons the potential shim locations have to be restricted to the area of the permanent magnet array. This necessitates the inclusion of both distributions (m_y and m_z) for an adequate minimization of the field integrals.

Further geometrical constraints are introduced to simplify the shimming procedure. The discretization of the shim positions in z-direction and the restriction of the shims to a fixed shape and a definite y-position allows for the determination of the shim thicknesses solving a set of linear equations. Otherwise, more sophisticated (and time consuming) minimization procedures have to be applied.

These constraints limit the accuracy of compensation. Fig. 9 gives an overview of the errors introduced by various constraints. The field of a
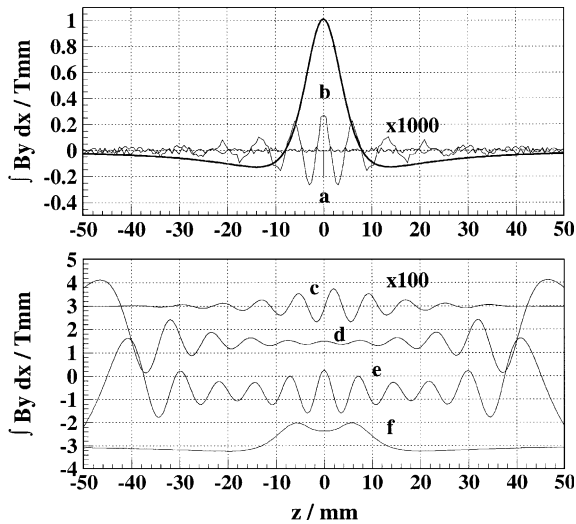
Fig. 9. A point dipole located 8 mm above the midplane pointing vertically gives a field integral as shown in the top panel (thick line). Residuals of various fits with shim magnets using the arrays described in the text are shown. The shim magnets have vertical magnetization and the vertical position corresponds to a gap of 15 mm. The residuals are multiplied by 1000 (top) and 100 (bottom). (a) Square magnets with a cross-section of 1×1 mm^2 at the location of the dipole error compensate the error nearly perfectly. In the following graphs square magnets with a cross-section of 4×4 mm^2 have been used. (b) The point dipole is located 9.5 mm above midplane. (c) The dipole is displaced by 2 mm in horizontal direction. (d) The dipole is displaced by 10 mm in vertical direction. (e) The dipole points in horizontal direction. (f) The strength of the magnets is discretized in steps of 0.02 of the unit volume of $4 \times 4 \times 4$ mm^3. Curves (c)–(f) are vertically shifted for clarity.

single dipole located 8 mm above the axis (top panel, thick line) is modelled by various distributions of correcting shims. The corresponding residuals are displayed.

The discretization of the shim distribution results in an oscillatory behavior of the residuals. Oscillations occur when the discretization for the shim thicknesses is too coarse (Fig. 9b), when the error dipole is located between shim grid positions (Fig. 9c), when the vertical positions of error dipole and shim are different (Fig. 9d), when an error dipole moment is compensated with shims of perpendicular magnetization direction (Fig. 9e) and when the discretization of the shim strength is too coarse (Fig. 9f). The amplitude of the oscillations decreases for finer grids but at the same time the frequency of the oscillations increases.

References

[1] S. Sasaki, Nucl. Instr. and Meth. A 347 (1994) 83.
[2] J. Bahrdt, W. Frentrup, A. Gaupp, P. Kuske, M. Scheer, W. Gudat, G. Ingold, S. Sasaki, Nucl. Instr. and Meth. A 467–468 (2001) 21.
[3] F. Schäfers, H.-Ch. Mertins, A. Gaupp, W. Gudat, M. Mertin, I. Packe, F. Schmolla, S. DiFonzo, G. Soullie, W. Jark, R.P. Walker, X. LeCann, R. Nyholm, M. Eriksson, Appl. Opt. 38 (1999) 4074;
M. Weiss, K. Sawhney, R. Follath, H.-Ch. Mertins, F. Schäfers, W. Frentrup, A. Gaupp, M. Scheer, J. Bahrdt, F. Senf, W. Gudat, in: P. Pianetta, J. Arthur, S. Brennan (Eds.), Proceedings of the 11th National Conference on Synchrotron Radiation Instrumentation (SRI1999), Stanford, USA, AIP, New York, CP521, 2000, pp. 134–136;
M.R. Weiss, R. Follath, K.J.S. Sawhney, F. Senf, J. Bahrdt, W. Frentrup, A. Gaupp, S. Sasaki, M. Scheer, H.-Ch. Mertins, D. Abramsohn, F. Schäfers, W. Kuch, W. Mahler, Nucl. Instr. and Meth. A 467–468 (2001) 449.
[4] T. Tanaka, T. Seike, H. Kitamura, Nucl. Instr. and Meth. A 465 (2001) 600.
[5] T. Tanaka, H. Kitamura, Rev. Sci. Instr. 71 (2000) 3010.
[6] A.D. Cox, B.P. Youngman, SPIE 582 (1986) 91.
[7] B.L. Bobbs, et al., Nucl. Instr. and Meth. A 296 (1990) 574.
[8] G. Ingold, T. Schmidt, Annual Report, SLS, Switzerland 2002.
[9] D.C. Quimby, S.C. Gottschalk, F.E. James, K.E. Robinson, J.M. Slater, A.S. Valla, Nucl. Instr. and Meth. A 285 (1989) 281;
S.C. Gottschalk, D.C. Quimby, K.E. Robinson, J.M. Slater, Nucl. Instr. and Meth. A 296 (1990) 579;
B. Diviacco, R.P. Walker, Nucl. Instr. and Meth. A 368 (1996) 522;
P. Elleaume, et al., Synchrotron Radiat. News 8 (1) (1995) 18.
[10] S. Marks, J. DeVries, E. Hoyer, B.M. Kincaid, D. Plate, P. Pipersky, R.D. Schlueter, A. Young, Proceedings of the 1999 Part. Acc. Conference, New York, NY, USA, 1999, pp. 162–164.
[11] Ch. Wang, L.H. Chang, C.H. Chang, M.C. Lin, C.-S. Hwang, J.-R. Chen, J. Synchrotron Radiat. 5 (1998) 478.
[12] J. Chavanne, P. Elleaume, P. Van Vaerenbergh, Proceedings of the 1999 Particle Acceleration Conference, New York, NY USA, 1999, pp. 2665–2667.
[13] P. Elleaume, O. Chubar, J. Chavanne, Proceedings of the 1997 Particle Acceleration Conference, Vancouver, Canada, 1997, pp. 3509–3511;
O. Chubar, P. Elleaume, J. Chavanne, J. Synchrotron Radiat. 5 (1998) 481.
[14] E. Hoyer, S. Marks, P. Pipersky, R. Schlueter, Rev. Sci. Instr. 66 (1995) 1901.
[15] P. Kuske, R. Görgen, J. Kuszynski, Proceedings of the 2001 Particle Acceleration Conference, Chicago, IL, USA, 2001, pp. 1656–1658.
[16] K. Halbach, Nucl. Instr. and Meth. 169 (1980) 1.
[17] B. Diviacco, R. Walker, Nucl. Instr. and Meth. A 292 (1990) 517.